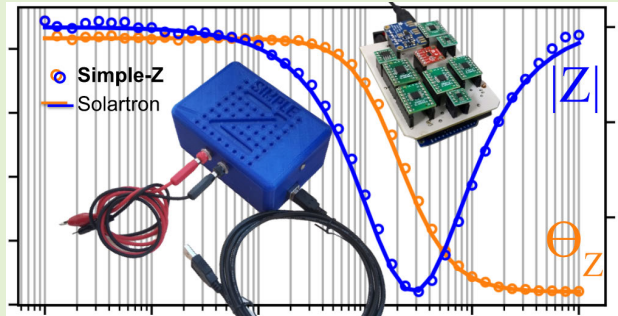


Simple-Z: A Low-Cost Portable Impedance Analyzer

Lorenzo A. Buscaglia^{ID}, João Paulo Carmo^{ID}, and Osvaldo N. Oliveira Jr.^{ID}

Abstract—The use of electrical impedance spectroscopy in point-of-care systems or for online monitoring has been hampered by the high cost of typical benchtop impedance analyzers. In this article, we introduce a portable, low-cost impedance analyzer, referred to as “Simple-Z,” which contains a signal processing unit that allows for a precise generation and reading of the excitation and response signals. Simple-Z is based on the integrated circuit AD5933 in conjunction with peripheral circuits for a fine output amplitude regulation, flexible response amplification, sampling rate control, automatic calibration, and external communication. Software solutions were implemented, including the strategical register overflow to allow decreasing frequency sweeps, the control of the number of acquisition cycles to reduce the spectral leakage of the discrete Fourier transform (DFT), and the iterative approximation for defining proper response amplification and calibration resistances. The software also included a graphical user interface (GUI) with entries, buttons, and graphs that allow for an intuitive usage of the device. Results generated with Simple-Z in equivalent circuits mimicking sensing systems and in aqueous solution of different Na_2SO_4 concentrations were essentially identical to those obtained with a commercial benchtop impedance analyzer. Since the cost of the circuitry and components to fabricate an instrument is near U.S. \$100 and because Simple-Z was designed to allow for easy upscale to mass production, one may expect it to be deployed in point-of-care diagnosis systems. Furthermore, it can also be used in teaching laboratories for training students in electrical impedance spectroscopy.

Index Terms—AD5933, biosensing, biosensor, calibration, electronic, impedance analyzer, impedance spectroscopy, sensor, signal processing, Simple-Z.



I. INTRODUCTION

ELECTRICAL impedance spectroscopy has been utilized in a variety of applications from materials characterization to clinical diagnosis using biosensors [2], [3]. Among other features, impedance spectroscopy allows for distinguishing from interface and bulk phenomena, which is useful particularly for (bio)sensing as the sensing units are made with nanomaterials and biomolecules that are sensitive to interface

effects [4]. The use for bio(sensing) of electrical impedance spectroscopy, and its counterpart in electrochemistry (electrochemical impedance spectroscopy), has been reviewed in [2] and [5], where their main advantages are highlighted. These advantages include high sensitivity as the electrical properties at liquid interfaces, including liquid–solid interfaces, are highly dependent on the microenvironment [6], [7]. Indeed, any small change in the electrolyte composition or on the ultrathin films of the sensing units is captured with impedance spectroscopy, especially because one may probe the electrical response at distinct frequencies. The electrical response in such sensors is governed by distinct mechanisms depending on the frequency. At high frequencies, above 10^5 Hz, the response is mostly due to capacitive effects, while at intermediate frequencies—around 10^3 Hz—the response depends on the film properties. At low frequencies, 10^2 Hz and below, the response depends mostly on double layer effects [8]. This frequency dependence allows for ample opportunities of feature selection to process impedance data, as it has been exploited with machine learning methods [9], [10]. Sensing with impedance spectroscopy today affords sensitivity and selectivity comparable to more sophisticated methods, including polymerase chain reaction (PCR) or enzyme linked immunosorbent assay (ELISA) [11]. Research into this area is

Manuscript received 16 August 2023; accepted 30 August 2023. Date of publication 11 September 2023; date of current version 31 October 2023. This work was supported in part by the Coordination of Superior Level Staff Improvement (CAPES), in part by the National Council for Scientific and Technological Development (CNPq) under Grant 304312/2020-7, in part by the National Institute of Organic Electronics (INEO), and in part by the São Paulo Research Foundation (FAPESP) under Grant 2018/22214-6 and Grant 2019/00101-8. The associate editor coordinating the review of this article and approving it for publication was Prof. Benoit Gosselin. (Corresponding author: Lorenzo A. Buscaglia.)

Lorenzo A. Buscaglia and Osvaldo N. Oliveira Jr. are with the Bernhard Gross Polymers Group, Department of Physics and Materials Science, São Carlos Institute of Physics, University of São Paulo, São Carlos 13560-970, Brazil (e-mail: lorenzo.buscaglia@gmail.com; chu@ifsc.usp.br).

João Paulo Carmo is with the Department of Electrical Engineering, São Carlos School of Engineering, University of São Paulo, São Carlos 13560-970, Brazil (e-mail: jcarmo@sc.usp.br).

Digital Object Identifier 10.1109/JSEN.2023.3312039

TABLE I
IMPEDANCE ANALYZERS COMPARISON

Device	Author	Year	US\$	Hz	Ω	V (AC)	Applications	Max. Error
*	Hoja and Lentka [16]	2010	*	10m – 100k	10 – 10G	100m – 1 **	Technical Objects	Z 1.6% θ 0.6%
*	Bogóñez-Franco et al. [17]	2010	*	100 – 200k	10 – 1k	100m – 1 **	Bioimpedance	Z 2.5% θ 4.5%
*	Chabowski et al. [18]	2015	*	1 – 100k	10 – 10M	100m – 1 **	Biological	Z 3.5% θ 2.8°
ABE-Stat	Jenkins et al. [19]	2019	~ 105	100m – 100k	100 – 100k	10m – 100m **	Agriculture & Food	***
*	Ibba et al. [20]	2021	*	10 – 100k	*	100m – 1 **	Agriculture On-field	Z 1.2% θ 3.8°
*	Istanbulu and Avci [21]	2021	*	10k – 100k	1k – 200k	100m – 1 **	Biomedical	Z 1.63% θ *
PModIA	Digilent (NI)	*	~ 40	1k – 100k	*	100m – 1 **	*	*
Eval-AD5933	Analog Devices	*	~ 70	1k – 100k	*	100m – 1 **	*	*
Sensit Smart	Palmsens BV	*	~ 1k	16m – 200k	*	1m – 250m	*	*
1260A	Solartron / Ametek	*	> 10k	10 μ – 32M	100m – 100T	0 – 3	General Purpose	Z 0.1% θ 0.1°
Simple-Z	Buscaglia [1]	2022	~ 100	1 – 100k	100 – 1M	10m – 1	Biosensing	 Z 1% θ 1°

* No data ** Only 4 options *** Discontinuities issue

normally done using benchtop instruments (not portable), such as Solartron 1260A (Ametek), E4990A (Keysight), and MFIA (Zurich Instruments), whose cost is above U.S. \$10 000. It is possible, nevertheless, to perform experiments with portable instruments, thus permitting the development of biosensing platforms within the point-of-care paradigm [10], [12]. This has been mostly explored with potentiostats, for which commercial instruments have been made available for some time by brands, such as Metrohm and PalmSens, among others. Furthermore, homemade potentiostats have also been reported [13], [14], [15]. The same does not apply to impedance spectroscopy as only recently have commercial impedance analyzers become available in “portable” models, however not yet wireless or self-powered. One example is Sensit Smart (PalmSens), but its cost is still relatively high (>U.S. \$1000) for deploying in point-of-care systems.

To the best of our knowledge, the first published attempts of developing a low-cost wide-spectrum impedance analyzer were in 2010 [16], [17]. They were based on the integrated circuit AD5933 (Analog Devices), which provides some basic signal processing functions for a highly competitive price (~U.S. \$20). Since then, multiple strategies have been employed, separately, to increase amplitude, frequency, and impedance ranges, as well as precision and user experience, among other limitations of AD5933 [18], [19], [20], [21]. However, only costly commercial alternatives met all biosensing requirements simultaneously. Approaches using low-cost (~U.S. \$30) field-programmable gate arrays (FPGAs) do not exempt the need for an external analog front-end for amplifications, calibration, conversions, and filtering, aside from being only adequate for low production volumes (up to 1000 units) [22], [23], [24], [25], [26]. Furthermore, the

commercially available FPGAs that include an internal oscillator (OSC) are much more expensive. With the aim of making it possible to employ sensors and biosensors based on impedance spectroscopy in point-of-use settings, we developed Simple-Z: a portable, precise, and low-cost impedance analyzer. Table I presents a comparison between some impedance analyzers, including Simple-Z, considering features, performance, and cost. Complementary tables can be found in [18], [19], [20], and [27]. Beyond merging ideas implemented in the literature, our design includes new strategies for output and response amplitude regulation, discrete Fourier transform (DFT) calculation, and impedance calibration, among others. The system is divided into three parts: the signal processing unit, which generates the excitation and reads the response; the sensing unit(s), which interacts physicochemically with the sample; and the data analysis unit, which classifies the spectra obtained.

II. DESIGN OF THE ELECTRONIC CIRCUITRY

The central component of the impedance analyzer is the integrated circuit AD5933, which comprises an output frequency generation, output amplification, response amplification, impedance readout, calibration, and communication. Particularly for sensing, these AD5933 components had limitations that were overcome in the design of Simple-Z, with the electronic diagram shown in Fig. 1. This diagram uses color blue for AD5933 embedded circuitry (arrows define digital signal flux), black for the external circuitry implemented in this project, orange for units outside Simple-Z, and green for the circuit functional groups described in Sections II-A–II-F (dashed green lines connect distant parts of the same functional group).

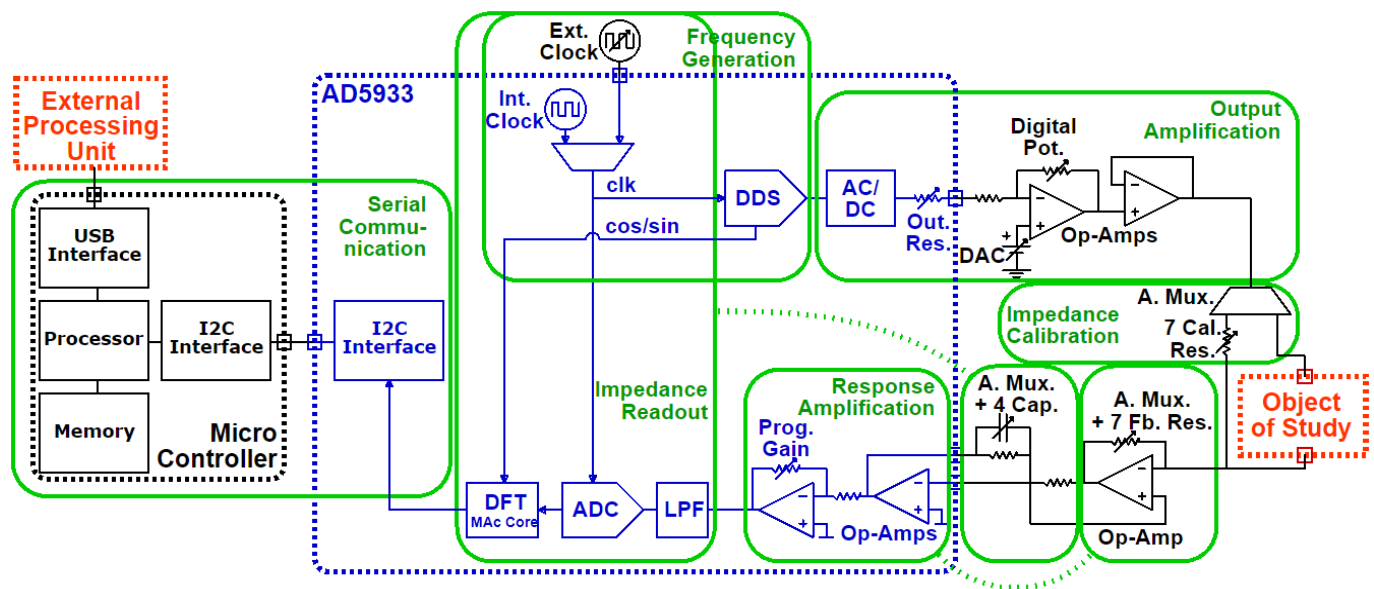


Fig. 1. Electronic diagram of Simple-Z. Source: adapted from [1].

A. Frequency Generation

AD5933 contains a direct digital synthesizer (DDS) shown in Fig. 1, which generates a sinusoidal signal with digitally controlled frequency defined by a programmable 24-bit frequency control register (FCR) and 16.776-MHz internal OSC. A 27-bit phase accumulation register (PAR) accumulates FCR at OSC rate and provides its first bits as address for the digital-to-analog converter (DAC) to access one of the equally spaced sine values in its lookup table (LUT). PAR truncates after sufficient accumulations, resulting in an organized and cyclic conversion of the sinusoidal values inside LUT at a rate established by OSC and with (memory) steps established by FCR. The list of frequencies to be analyzed is defined by programming the registers for the initial frequency, the frequency step size, and number of steps, implying increasing order and linear separation. The frequency changes through a “frequency increment” command, which adds to FCR the value inside a 24-bit frequency increment register (FIR), meaning the frequency cannot be directly reduced. However, performing this command sufficient times permits overflowing the FCR and obtaining decreasing frequency order, vastly utilized in the literature for impedance spectroscopy. Varying the FIR value before each “frequency increment” also allowed for logarithmic separation, useful for measurements involving multiple frequency decades. Both solutions were implemented in software.

B. Output Amplification

Four options are provided by AD5933 for output ac amplitude (50, 100, 500, and 1000 mV), with distinct dc amplitudes (200, 300, 750, and 1500 mV, respectively). Several limitations appear with these values, since in some biosensing applications, ac amplitudes down to 10 mV are required. A second issue is the lack of control over the dc amplitude, which can impact polarization and produce unwanted chemical reactions, besides complicating the processing of the response signal.

The first ac amplitude limitations were solved with a negative feedback variable amplification using an operational amplifier (OP-AMP) AD8606 coupled with an 8-bit (256 positions) digital potentiometer AD5252. This, combined with the four amplitude options given by AD5933, resulted in an ac amplitude range from 10 to 1000 mV, with resolution going from 2% (0.2 mV) for the lowest and 0.4% (4 mV) for the highest amplitudes. The dc amplitude issue was solved through using a 12-bit DAC MCP4725 output as “virtual ground,” connected to the positive OP-AMP input, in the former amplification. This approach permitted suppressing the dc amplitude (0 V). Another limitation of AD5933 is its low current limit, which constrains the impedance range to values over 1 k Ω . We used the secondary OP-AMP inside AD8606 in “follower” mode to allow for measuring impedances down to 100 Ω . The resulting circuit is shown in Fig. 1.

C. Response Amplification

For acquiring the response signal, AD5933 provides an analog-to-digital converter (ADC) ranging between ground (GND, 0 V) and supply voltages (V_{DD} , 3.3 V), with a 12-bit resolution (4096 positions). A successful acquisition of any ac signal requires its amplitude to be smaller than the conversion range (<3300 mV) to avoid voltage saturation. Also, the signal should be considerably larger than the maximum resolution ($\gg 0.8$ mV) to avoid a flat or deformed reading. These requirements imply the need to amplify the response amplitude, which depends on the excitation amplitude and on the unknown impedance (Z) magnitude. AD5933 provides a first amplification stage based on an external feedback resistance (R_{FB}) to be chosen by the user for the Z range of a specific application. Additionally, it provides a two-option ($1\times$ or $5\times$) programmable gain (K_{PGA}) to cover small variations in Z without having to replace R_{FB} . However, these features are not sufficient for a versatile impedance analyzer. In Simple-Z, the output signal is programmable between

10^1 and 10^3 mV (two decades) to measure impedances between 10^2 and 10^6 Ω (four decades). Therefore, the response amplitude can vary within several decades for different applications. To multiply the choices of R_{FB} , we introduced the 8-to-1 analog multiplexer ADG728 (Analog Devices) with seven options for R_{FB} , as in Fig. 1. Combined with K_{PGA} , it resulted in 13 logarithmically distributed amplification options. Furthermore, an iterative software solution was developed to find the appropriate response amplification automatically for an unknown Z .

D. Impedance Readout

The correlation of the impedance with its excitation voltage and response current can be given by

$$Z = V_{EXC}/I_{RES}. \quad (1)$$

The AD5933 microdevice measures the current through the autobalanced bridge mentioned in Section II-C, which follows the equation:

$$V_I = R_{FB} \cdot I_{RES}. \quad (2)$$

Because of its linearity, AD5933 uses the DFT for the acquisition of I_{RES} based on the following equation:

$$\text{DFT}(I_{RES}) = \text{DFT}(V_I)/R_{FB}. \quad (3)$$

Equation (3) comprises a multiply-accumulation core, which performs a single-frequency DFT using 1024 sequential ADC acquisitions performed at 1/16 of the OSC frequency. This method may lack precision due to three main reasons: spectral leakage, undersampling, and interference. To mitigate leakage, we developed a cost-effective solution that relies on distributing the acquisition along several signal cycles (>10), thus “diluting” the leakage. Since distributing 1024 acquisition points along too many cycles can lead to undersampling issues, we established a maximum number of cycles for the acquisition length ($<10^2$). We used the programmable clock Si5351 (Silicon Laboratories) as an external OSC for AD5933, as presented in Fig. 1. A different OSC frequency was implemented for each decade of signal frequency, allowing for a wide measurement range (from 1 to 10^5 Hz). This solution led to interference by the top-flat shape of the sinusoidal wave created by DDS in the DFT calculation, which introduces unwanted harmonics. The reconstruction low-pass filter (LPF) embedded in AD5933 is only useful for high frequencies of the OSC. For low frequencies, we built an external variable reconstruction LPF based on a second ADG728 that establishes a five-option (one for each decade) first-order active LPF, as shown in Fig. 1. The capacitance and resistance values were chosen to filter all frequencies above the maximum signal frequency of each decade. The resultant time constant of the filters was around 0.15% of the total acquisition time, for all frequencies, thus insignificantly affecting the results.

E. Impedance Calibration

For measuring the excitation voltage V_{EXC} , the datasheet of AD5933 recommends manual replacement of Z with a calibration resistance R_{CAL} and then repeating the measurement procedure.

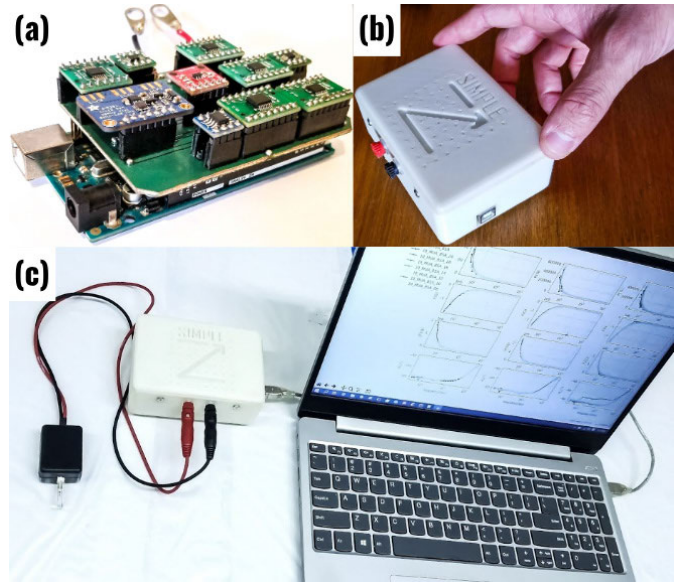


Fig. 2. Simple-Z (a) fabricated circuit, (b) fully mounted, and (c) connected for sensing. Source: adapted from [1].

This leads to

$$V_V = -(R_{FB}/R_{CAL}) \cdot V_{EXC} \quad (4)$$

onto which a DFT can be applied, resulting in the following equation:

$$\text{DFT}(V_{EXC}) = -(R_{CAL}/R_{FB}) \cdot \text{DFT}(V_V). \quad (5)$$

With this second DFT result, the complex impedance can be obtained through

$$Z = R_{CAL} \cdot \text{DFT}(V_V) \cdot \text{DFT}(I_{RES}). \quad (6)$$

The precision of this calculation depends strongly on the proximity of R_{CAL} to the magnitude of Z , which is a problem when the aim is a versatile analyzer with a wide impedance range. In our approach, we used $\text{DFT}(I_{RES})$ for a rough estimation of Z magnitude and then replacing Z with the corresponding R_{CAL} using a third ADG728 with seven calibration resistances, introduced in Fig. 1, logarithmically distributed from 10^2 to 10^6 Ω .

F. Serial Communication

AD5933 only includes memory for storing a single DFT result, in two (real and imaginary) 16-bit registers. For spectroscopy to be performed, AD5933 includes an I²C serial interface that allows for communicating the values inside these registers to a microprocessor, which can store and process them. The I²C protocol uses two connections: a timing reference and a data channel. These connections are shared between several integrated circuits inside Simple-Z, once I²C assigns a unique address to each. However, computers required for processing the impedance spectra normally use universal serial bus (USB) protocols. To bridge between these technologies, we employed the microcontroller Arduino Mega 2560 with I²C and USB interfaces, as in Fig. 1. It also provides sufficient memory to store the electrical impedance spectroscopy

algorithm, which yields multiple integrated circuits and to perform a preprocessing of the measurement data before communicating it to the computer.

III. MANUFACTURING

The first prototyping steps were taken using stripboards to accelerate the circuit fabrication process. For the final prototype, a printed circuit board (PCB) was designed using the EasyPCB software. The surface-mount devices (SMD) ICs were soldered onto dual in-line package (DIP) adaptors to simplify their replacement. The microcontroller was assembled under it to reduce horizontal dimensions, as shown in Fig. 2(a). The PCB was fabricated with the traditional method of selective corrosion for a double-sided copper-clad laminate, involving photosensitive ink painting, selective UV curing, noncured ink removal, and corrosion of exposed copper. The casing was designed in Autodesk Inventor software and fabricated with 1.75-mm white polylactic acid (PLA) filament in a GTMax3D printer. It allowed protection to moisture, dust, unwanted electrical contacts, and small impacts. The casing has one opening for USB connection, two for analog connections (red and black), and its logo inscribed at the top, as can be seen in Fig. 2(b) and (c). The whole system, including ICs, casing, and connections, had a cost near U.S. \$100.

IV. SOFTWARE

The system comprises a sequential algorithm stored in the microcontroller memory, responsible for executing the electrical impedance spectroscopy measurement steps. This algorithm was developed in C++ language in Arduino IDE, as summarized in the flowchart of Fig. 3. The “settling” refers to the number of signal cycles to wait before starting the acquisition, useful to avoid transient phenomena. Considering zero settling time, points in the first frequency decade take a minimum of 20 s to be measured, due to the minimum number of measurement cycles, which get repeated during the calibration process. This required time is reduced ten times in each of the following decades, giving an idea of the total time of a spectroscopy, depending on the desired parameters. In practice, during our experiments, it resulted slightly faster than Solartron 1260A.

A second algorithm is executed simultaneously in the computer, responsible for interacting with the user, thus event-driven with a graphical user interface (GUI). This algorithm was developed using Python language with Tkinter (<https://docs.python.org/3/library/tkinter.html>) and included buttons, text entries, and graphs, which can be seen in Fig. 4. It is worth noting that the settling period can be set in cycles or milliseconds; however, ultimately Simple-Z transforms the milliseconds into the correspondent (rounded) cycles for each frequency, having a maximum (2044 cycles) established by AD5933.

V. RESULTS

The possible reproducibility in manufacturing was verified through the fabrication of four additional instruments, which

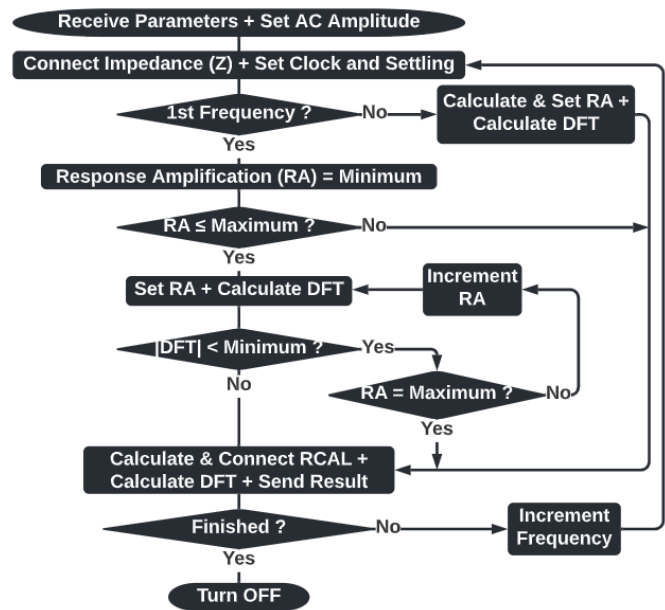


Fig. 3. Flowchart of the sequential impedance spectroscopy algorithm of Simple-Z. Source: adapted from [1].

are shown in Fig. 5. They had the cases of different colors and PCBs obtained from JLCPCB Company. Each case took 5 h to fabricate, while the manual soldering of each PCB was a 7-h process. Although the number of instruments fabricated is small, the reproducibility of their results indicates that mass production of Simple-Z is feasible. In particular, 3-D printing can be accelerated (down to seconds) using the injection technology, and the soldering time can also be diminished (down to minutes) with the surface-mount technology.

The error and the standard deviation of Simple-Z results were measured through a comparison with the commercial impedance analyzer Solartron 1260A. Since (bio)sensors have a considerable standard deviation, we opted for using high-precision resistors and capacitors to build four equivalent circuits, whose electrical response would approximately correspond to those of human tissues. Obtained from the literature and adapted for the commercial values available, they included a Cole–Cole model for biceps [28] and circuits for breast cancer cells [29], blood [30], and forearm [31]. The circuits diagrams can be observed at the top panels of Fig. 6. We performed 3 measurements with each circuit, ranging between 1 and 10^5 Hz with 500-mV amplitude. The average Bode plots for the 4 cases, also at the top panels of Fig. 6, indicate the similarity in response for Solartron 1260A (solid line) and Simple-Z (circles). The differences (dif) between these devices are shown in the middle panels of Fig. 6. The magnitude is represented in percentage, as relative difference, by dividing the difference by Simple-Z’s measured average magnitude. It is significant that the maximum impedance magnitude deviation is ca. 8%, staying mostly under 2%, and the maximum phase deviation is ca. 6° , being mostly below 2° . Most impedance-based detections use relative variation against a reference or “blank”, which means that random deviations

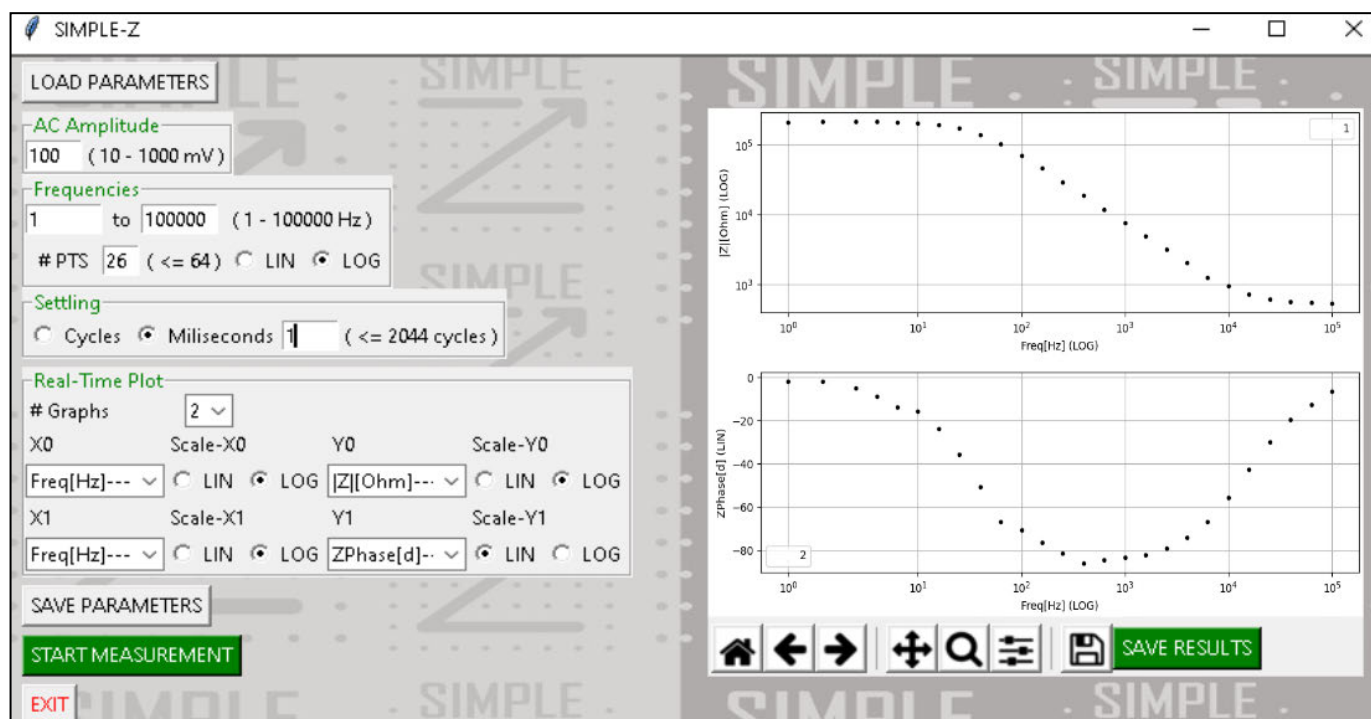


Fig. 4. Screenshot of Simple-Z's GUI. Source: adapted from [1].



Fig. 5. Five copies of Simple-Z. Source: adapted from [1].

are more compromising than comparative errors. The standard deviations (std) of the triplicated measurements of Simple-Z are shown in the bottom panels of Fig. 6, being less than 1% (relative standard deviation) in magnitude and 1.5° in phase. The power consumption of the device was monitored using a Kewesi USB current meter and resulted in 0.45 W (0.09 A) in the standby mode and 0.55 W (0.11 A) during measurements, independently of the frequency, amplitude, and impedance values.

Among all the parameters that may affect the impedance of a solution, the concentration of electrolytes may be the most relevant. As a proof of concept, we aimed to quantify sodium sulfate (Na_2SO_4), and we again compared the results of Simple-Z and Solartron 1260A. We used gold interdigitated microelectrodes that consisted in 50 pairs of digits $10 \mu\text{m}$ wide and spaced over a BK7 glass substrate. These were

fabricated at the Brazilian National Center of Research in Energy and Materials (CNPEM) using photolithography. The measurements used 200-mV ac amplitude ranging between 2.5 Hz and 16 kHz with nine concentrations of Na_2SO_4 (10^{-3} to 10 mg/mL) and 30- μL samples. The spectra obtained with both devices are almost identical in most of the frequency range, as can be seen in Fig. 7. This sensing application, complemented with the validation using RC circuits, suggested the compatibility of Simple-Z for measurements with biological objects. For practical purposes, its utility in a real-time (bio)sensing application was demonstrated in a recent article using a genosensor to detect SARS-CoV-2 genetic sequence with a limit of detection of 0.5 aM [11]. Furthermore, different units of Simple-Z have been used in detecting biomarkers and bacteria in fluids, such as phosphate buffered saline solution (PBS) and milk.

VI. CONCLUSION

In this work, we developed a palm-sized, low-cost impedance analyzer referred to as Simple-Z. We used the integrated circuit AD5933, which is a suitable option available commercially for combining a DDS with a digital DFT calculator. We developed additional circuits to overcome several limitations of AD5933 toward automated measurements. Simple-Z is made 100% of off-the-shelf components with a total cost near U.S. \$100, which is currently more than ten times cheaper than any commercial alternative. It works with wide ranges of impedance magnitude (10^2 to $10^6 \Omega$), alternated current amplitude (10^{-2} to 1 V), and frequency (1 to 10^5 Hz) and includes a GUI. A performance analysis was done using human tissue-equivalent circuits made of resistors and capacitors, resulting in impedance deviations under 1% in magnitude and 1.5° in phase. Its functionality was validated

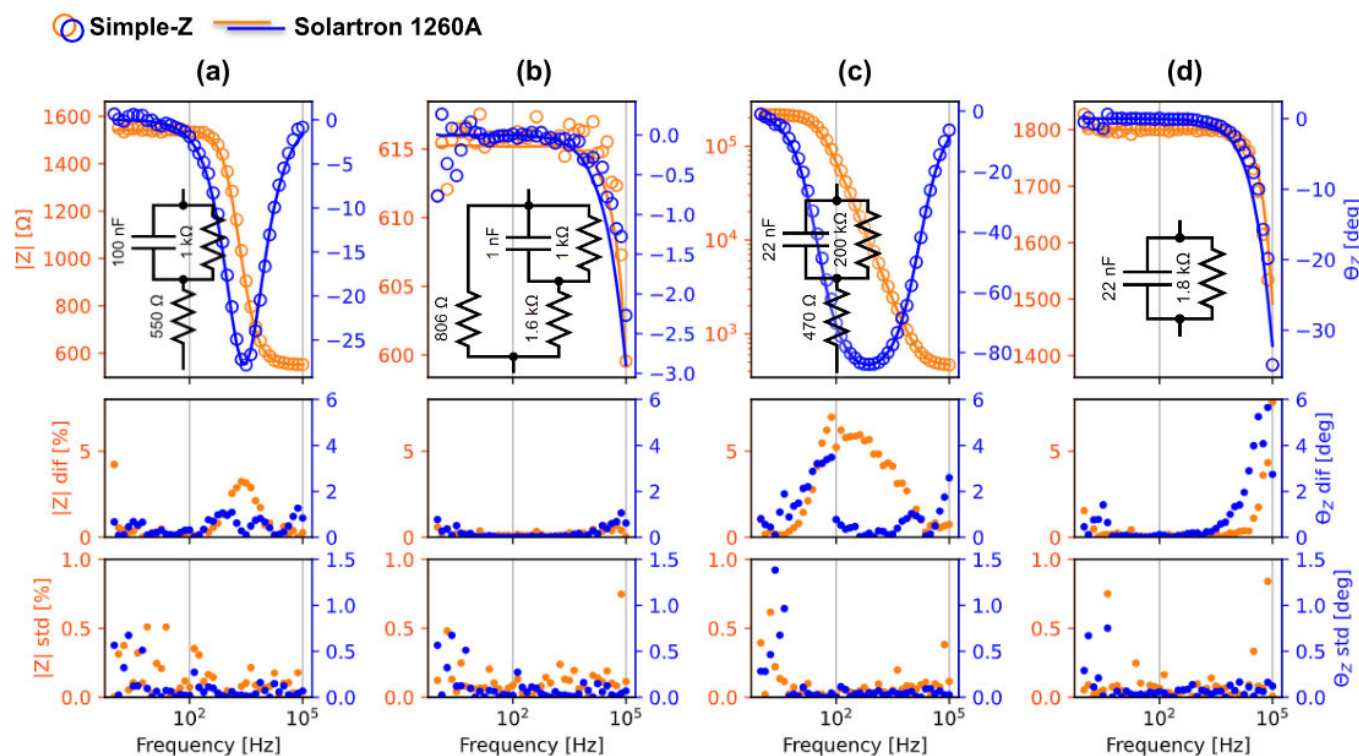


Fig. 6. Bode plots measured with (circles) Simple-Z and (solid line) Solartron from equivalent circuits for (a) biceps Cole–Cole model [28], (b) breast cancer cells [29], (c) blood [30], and (d) forearm [31] (top), impedance difference (middle), and standard deviation of Simple-Z (bottom). Source: adapted from [1].

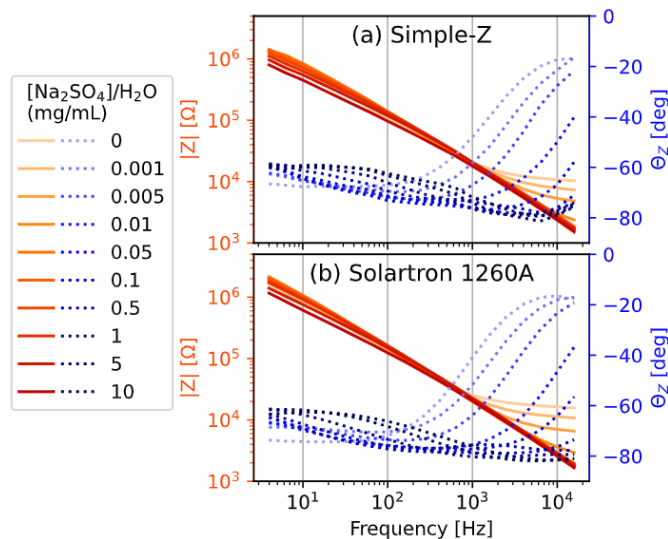


Fig. 7. Bode spectra of ten concentrations of Na_2SO_4 in pure water measured with (a) Simple-Z and (b) Solartron 1260A. Source: adapted from [1].

in a biosensing work for detecting SARS-CoV-2. Five units of Simple-Z were fabricated to be used by the researchers of our group. It represents a bridge over the technological gap between the proof-of-principle experiments with biosensors and the development of integrated prototypes to be applied in the field. We envisage that Simple-Z will be useful for applications in (bio)sensing, as demonstrated here, and in

teaching laboratories of universities. Nowadays, impedance spectroscopy experiments are not normally performed in teaching at undergraduate level owing to the high cost of providing dozens of instruments at once for a class of students. With Simple-Z, this will be feasible.

REFERENCES

- [1] L. A. Buscaglia, “Development of a portable impedance spectrometer,” M.S. thesis, Dept. Phys. Mater. Sci. (FCM), Univ. Sao Paulo, Sao Carlos, Brazil, 2022, doi: 10.11606/D.76.2022.tde-19072022-120227.
- [2] L. A. Buscaglia, O. N. Oliveira, and J. P. Carmo, “Roadmap for electrical impedance spectroscopy for sensing: A tutorial,” *IEEE Sensors J.*, vol. 21, no. 20, pp. 22246–22257, Oct. 2021, doi: 10.1109/JSEN.2021.3085237.
- [3] H. Caytak, A. Boyle, A. Adler, and M. Bolic, “Bioimpedance spectroscopy processing and applications,” in *Encyclopedia of Biomedical Engineering*, vol. 3. New York, Ny, USA: Elsevier, 2019, doi: 10.1016/B978-0-12-801238-3.10884-0.
- [4] O. N. Oliveira, R. M. Iost, J. R. Siqueira, F. N. Crespilho, and L. Caseli, “Nanomaterials for diagnosis: Challenges and applications in smart devices based on molecular recognition,” *ACS Appl. Mater. Interfaces*, vol. 6, no. 17, pp. 14745–14766, Sep. 2014, doi: 10.1021/am5015056.
- [5] E. P. Randviir and C. E. Banks, “A review of electrochemical impedance spectroscopy for bioanalytical sensors,” *Anal. Methods*, vol. 14, no. 45, pp. 4602–4624, 2022, doi: 10.1039/d2ay00970f.
- [6] O. N. Oliveira and C. Bonardi, “The surface potential of Langmuir monolayers revisited,” *Langmuir*, vol. 13, no. 22, pp. 5920–5924, Oct. 1997, doi: 10.1021/la970272o.
- [7] D. M. Taylor, O. N. Oliveira, and H. Morgan, “Models for interpreting surface potential measurements and their application to phospholipid monolayers,” *J. Colloid Interface Sci.*, vol. 139, no. 2, pp. 508–518, 1990, doi: 10.1016/0021-9797(90)90123-6.
- [8] D. M. Taylor and A. G. Macdonald, “AC admittance of the metal/insulator/electrolyte interface,” *J. Phys. D, Appl. Phys.*, vol. 20, no. 10, pp. 1277–1283, Oct. 1987, doi: 10.1088/0022-3727/20/10/010.

- [9] T. J. Bondancia et al., "Low-cost bacterial nanocellulose-based interdigitated biosensor to detect the p53 cancer biomarker," *Biomaterials Adv.*, vol. 134, Mar. 2022, Art. no. 112676, doi: [10.1016/j.msec.2022.112676](https://doi.org/10.1016/j.msec.2022.112676).
- [10] A. Coatrini-Soares et al., "Microfluidic E-tongue to diagnose bovine mastitis with milk samples using machine learning with decision tree models," *Chem. Eng. J.*, vol. 451, Jan. 2023, Art. no. 138523, doi: [10.1016/j.cej.2022.138523](https://doi.org/10.1016/j.cej.2022.138523).
- [11] J. C. Soares et al., "Detection of a SARS-CoV-2 sequence with genosensors using data analysis based on information visualization and machine learning techniques," *Mater. Chem. Frontiers*, vol. 5, no. 15, pp. 5658–5670, 2021, doi: [10.1039/D1QM00665G](https://doi.org/10.1039/D1QM00665G).
- [12] J. L. Bott-Neto, T. S. Martins, L. A. Buscaglia, S. A. S. Machado, and O. N. Oliveira, "Photocatalysis of TiO₂ sensitized with graphitic carbon nitride and electrodeposited aryl diazonium on screen-printed electrodes to detect prostate specific antigen under visible light," *ACS Appl. Mater. Interfaces*, vol. 14, no. 19, pp. 22114–22121, May 2022, doi: [10.1021/acsami.2c03106](https://doi.org/10.1021/acsami.2c03106).
- [13] A. Ainla et al., "Open-source potentiostat for wireless electrochemical detection with smartphones," *Anal. Chem.*, vol. 90, no. 10, pp. 6240–6246, May 2018, doi: [10.1021/acs.analchem.8b00850](https://doi.org/10.1021/acs.analchem.8b00850).
- [14] S. C.-H. Lee and P. J. Burke, "NanoStat: An open source, fully wireless potentiostat," *Electrochimica Acta*, vol. 422, Aug. 2022, Art. no. 140481, doi: [10.1016/j.electacta.2022.140481](https://doi.org/10.1016/j.electacta.2022.140481).
- [15] M. D. Steinberg, P. Kassal, I. Kereković, and I. M. Steinberg, "A wireless potentiostat for mobile chemical sensing and biosensing," *Talanta*, vol. 143, pp. 178–183, Oct. 2015, doi: [10.1016/j.talanta.2015.05.028](https://doi.org/10.1016/j.talanta.2015.05.028).
- [16] J. Hoja and G. Lentka, "Interface circuit for impedance sensors using two specialized single-chip microsystems," *Sens. Actuators A, Phys.*, vol. 163, no. 1, pp. 191–197, Sep. 2010, doi: [10.1016/j.sna.2010.08.002](https://doi.org/10.1016/j.sna.2010.08.002).
- [17] P. Bogónez-Franco, A. Bayés-Genís, J. Rosell, and R. Bragós, "Performance of an implantable impedance spectroscopy monitor using ZigBee," *J. Phys., Conf.*, vol. 224, Apr. 2010, Art. no. 012163, doi: [10.1088/1742-6596/224/1/012163](https://doi.org/10.1088/1742-6596/224/1/012163).
- [18] K. Chabowski, T. Piasecki, A. Dzierka, and K. Nitsch, "Simple wide frequency range impedance meter based on AD5933 integrated circuit," *Metrolog. Meas. Syst.*, vol. 22, no. 1, pp. 13–24, Mar. 2015, doi: [10.1515/mms-2015-0006](https://doi.org/10.1515/mms-2015-0006).
- [19] D. M. Jenkins, B. E. Lee, S. Jun, J. Reyes-De-Corcuera, and E. S. McLamore, "ABE-stat, a fully open-source and versatile wireless potentiostat project including electrochemical impedance spectroscopy," *J. Electrochem. Soc.*, vol. 166, no. 9, pp. 3056–3065, Mar. 2019, doi: [10.1149/2.0061909jes](https://doi.org/10.1149/2.0061909jes).
- [20] P. Ibba et al., "Design and validation of a portable AD5933-based impedance analyzer for smart agriculture," *IEEE Access*, vol. 9, pp. 63656–63675, 2021, doi: [10.1109/ACCESS.2021.3074269](https://doi.org/10.1109/ACCESS.2021.3074269).
- [21] M. Istanbulu and M. Avci, "An ANN-based single calibration impedance measurement system for skin impedance range," *IEEE Sensors J.*, vol. 21, no. 3, pp. 3776–3783, Feb. 2021, doi: [10.1109/JSEN.2020.3022483](https://doi.org/10.1109/JSEN.2020.3022483).
- [22] J. Fe, R. Gadea-Gironés, J. M. Monzo, Á. Tebar-Ruiz, and R. Colom-Palero, "Improving FPGA based impedance spectroscopy measurement equipment by means of HLS described neural networks to apply edge AI," *Electronics*, vol. 11, no. 13, p. 2064, Jun. 2022, doi: [10.3390/electronics11132064](https://doi.org/10.3390/electronics11132064).
- [23] Z. Jiang et al., "Development of a portable electrochemical impedance spectroscopy system for bio-detection," *IEEE Sensors J.*, vol. 19, no. 15, pp. 5979–5987, Aug. 2019, doi: [10.1109/JSEN.2019.2911718](https://doi.org/10.1109/JSEN.2019.2911718).
- [24] H. Sohal, H. Wi, A. L. McEwan, E. J. Woo, and T. I. Oh, "Electrical impedance imaging system using FPGAs for flexibility and interoperability," *Biomed. Eng. OnLine*, vol. 13, no. 1, p. 126, Dec. 2014, doi: [10.1186/1475-925X-13-126](https://doi.org/10.1186/1475-925X-13-126).
- [25] A. Tsukahara, T. Yamaguchi, Y. Tanaka, and A. Ueno, "FPGA-based processor for continual capacitive-coupling impedance spectroscopy and circuit parameter estimation," *Sensors*, vol. 22, no. 12, p. 4406, Jun. 2022, doi: [10.3390/s22124406](https://doi.org/10.3390/s22124406).
- [26] X. Ye, T. Jiang, Y. Ma, D. To, S. Wang, and J. Chen, "A portable, low-cost and high-throughput electrochemical impedance spectroscopy device for point-of-care biomarker detection," *Biosensors Bioelectron.*, X, vol. 13, May 2023, Art. no. 100301, doi: [10.1016/j.biosx.2022.100301](https://doi.org/10.1016/j.biosx.2022.100301).
- [27] I. Showkat, F. A. Khanday, and M. R. Beigh, "A review of bio-impedance devices," *Med. Biol. Eng. Comput.*, vol. 61, no. 5, pp. 927–950, May 2023, doi: [10.1007/s11517-022-02763-1](https://doi.org/10.1007/s11517-022-02763-1).
- [28] T. J. Freeborn and G. W. Bohannon, "Changes of fractional-order model parameters in biceps tissue from fatiguing exercise," in *Proc. IEEE Int. Symp. Circuits Syst.*, May 2018, pp. 1–5, doi: [10.1109/ISCAS.2018.8351812](https://doi.org/10.1109/ISCAS.2018.8351812).
- [29] G. Qiao, W. Wang, W. Duan, F. Zheng, A. J. Sinclair, and C. R. Chatwin, "Bioimpedance analysis for the characterization of breast cancer cells in suspension," *IEEE Trans. Biomed. Eng.*, vol. 59, no. 8, pp. 2321–2329, Aug. 2012, doi: [10.1109/TBME.2012.2202904](https://doi.org/10.1109/TBME.2012.2202904).
- [30] F. Gómez, J. Bernal, J. Rosales, and T. Cordova, "Modeling and simulation of equivalent circuits in description of biological systems—A fractional calculus approach," *J. Electr. Bioimpedance*, vol. 3, no. 1, pp. 2–11, Jul. 2012, doi: [10.5617/jeb.225](https://doi.org/10.5617/jeb.225).
- [31] T. Dai and A. Adler, "In vivo blood characterization from bioimpedance spectroscopy of blood pooling," *IEEE Trans. Instrum. Meas.*, vol. 58, no. 11, pp. 3831–3838, Nov. 2009, doi: [10.1109/TIM.2009.2020836](https://doi.org/10.1109/TIM.2009.2020836).



Lorenzo A. Buscaglia was born in Bariloche, Argentina, in 1996. He received the Engineer degree in mechatronics and the M.Sc. degree in applied physics from the University of São Paulo (USP), São Carlos, Brazil, in 2018 and 2022, respectively.

He is a Founder and Main Researcher of the startup Blatron Tecnologia, São Carlos. He is specialized in electrical impedance spectroscopy techniques. He is interested mainly in the development of low-cost devices for sensing

and biosensing applications.



João Paulo Carmo was born in Maia, Portugal, in 1970.

He is a Professor at the University of São Paulo (USP), São Carlos, Brazil. He is involved in the research on micro/nanotechnologies, solid-state integrated sensors, and microdevices for biomedical and industrial applications.

Dr. Carmo is the Vice-Director of the Group of Metamaterials, Microwaves and Optics (GMeta).



Osvaldo N. Oliveira Jr. received the Ph.D. degree from Bangor University, Bangor, U.K., in 1990.

He is the Director of the São Carlos Institute of Physics, University of São Paulo, São Carlos, Brazil. He has led research into novel materials and has pioneered the combined use of statistical physics and artificial intelligence to process text and analyze sensing and biosensing data.

Prof. Oliveira is a member of the Latin American Academy of Sciences and Brazilian Academy of Sciences, the President of the International Union of Materials Research Society (IUMRS), and an Executive Editor of *ACS Applied Materials & Interfaces*.